

Received May 29, 2020, accepted June 23, 2020, date of publication July 14, 2020, date of current version August 13, 2020.

Digital Object Identifier 10.1109/ACCESS.2020.3009220

Finger-Vein Pattern Restoration With Generative Adversarial Network

SHUQIANG YANG^{1,4}, HUA FENG QIN², XIA LIU³, AND JUN WANG⁴

¹School of Physics and Electronic Information, Luoyang Normal University, Luoyang 471934, China

²School of Computer Science and Information Engineering, Chongqing Technology and Business University, Chongqing 400067, China

³College of Mobile Telecommunications, Chongqing University of Posts and Telecommunications, Chongqing 401520, China

⁴School of Information and Control Engineering, China University of Mining and Technology, Xuzhou 221000, China

Corresponding author: Huafeng Qin (qinhuafengfeng@163.com)

This work was supported in part by the National Natural Science Foundation of China under Grant 61976030 and Grant 61202063, in part by the Foundation for University Key Teacher by the Ministry of Education of Henan under Grant 2017GGJS136, in part by the Natural Science Foundation Project of Chongqing under Grant cstc2017jcyjAX0002, Grant cstc2018jcyjAX0095, and Grant cstc2017zdcy-zdyfx0067, and in part by the Scientific and Technological Research Program of the Chongqing Municipal Education Commission under Grant KJQN201900848, in part by the Chongqing Talent Plan under Grant CQYC201903246, and in part by the Educational Reform Research Project of the Chongqing Education Commission under Grant 201023 and Grant yig201016.

ABSTRACT Finger-vein recognition technology has attracted more and more attention because of its high security and convenience. However, the finger-vein image capturing is affected by various factors, which results that some vein patterns are missed in acquired image. Matching minutiae features in such images ultimately degrades verification performance of the finger-vein recognition system. To overcome this problem, in this paper, a novel finger-vein image restoration approach is proposed to recover the missed patterns based on generative adversarial network (GAN), as the first attempt in this area. Firstly, we employ the segmentation algorithm to extract finger-vein network, which is further subject to thinning operation. Secondly, the resulting thinning image is taken as an input of a GAN model to restore the missed vein patterns. Thirdly, the minutiae points are extracted from restoration finger-vein pattern. Finally, we propose a matching approach for verification. Experimental results show that the proposed method can restore the missed vein pattern and reduce the equal error rate (EER) of the finger-vein verification system.

INDEX TERMS Finger-vein recognition, vein restoration, generative adversarial network.


I. INTRODUCTION

With the rapid development and application of the Internet, people pay more and more attention to the security protection of individual identity. How to ensure the security and efficiency of recognition is a key problem in the information society. Biometrics authentication technologies as a solution have been widely investigated in past years. Currently, various biometrics traits such as fingerprints [1], faces [2], irises [3], and veins [4] have been applied for personal authentication and can be broadly categorized two categories [5]: (1) extrinsic traits such as face, fingerprint, iris, and gait; (2) intrinsic traits such as finger-vein, palm vein, and hand vein. Extrinsic traits are vulnerable to copy and fake, which results some concerns on privacy and security in practice. By contrast, intrinsic traits are hidden under the skin and

are difficult to be copy and forged, providing higher security and better privacy. Therefore, vein recognition has received increasing attentions.

The veins are located inside the skin. The finger-vein pattern extends from finger root to fingertip, and has clear network and good connectivity (as shown in Fig.1). In general, it is difficult to observe the finger-vein pattern in visible light. Different skin layers have different responses to infrared light, so we can collect the vein pattern using infrared light. Existing works [4], [6]–[8] have carried lots of experiments and the resulting experimental results imply that infrared illumination with wavelength of 850 nm are able to capture finger-vein images with high contrast.

For fingerprint recognition and finger knuckle recognition [9]–[12], the minutiae features such as bifurcation points and ending points have been employed as discriminative features and successfully applied for recognition because they have the advantage of low storage cost, low matching

The associate editor coordinating the review of this manuscript and approving it for publication was Peter Peer .

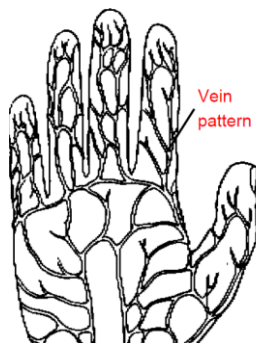


FIGURE 1. Vein pattern in the palm and fingers [35].

time cost and distinction. Similarly, the minutiae features of finger-vein patterns including bifurcation points and ending points as the common features are extracted for finger-vein recognition [13]–[16] and showed promising performance. In these approaches, the vein network is segmented and stored in a binary image and then the minutiae features are extracted from resulting binary image. Unfortunately, finger-vein image quality is inherently affected by a number of factors: environmental illumination [17]–[19], ambient temperature [4], [19], [20], light scattering in imaging finger tissues [21]–[24]. These factors are impossible to be controlled and/or avoided in practical applications, so the vein verification system generates some low quality images where the separability between the vein and non-vein patterns is poor or some vein patterns are corrupted. Therefore, the extracted vein network are generally not connective because some vein patterns are missed, which results incorrect minutiae features. In general, matching such minutiae features will ultimately degrade the performance of vein verification system. To overcome this problem, a lot of approaches have been proposed to restore the finger-vein pattern, showing good performance on different databases. They can be broadly classified into two categories such as image level and feature level [25]:

A. IMAGE LEVEL RESTORATION

Some image level restoration approaches [21] assume that biological tissue is highly heterogeneous and behaves as a multiple scattering medium in NIR imaging which results the low contrast and the sparse noise in the captured image. Therefore, many scattering removal approaches are proposed to improve the visibility restoration of vein images. For example, the work designs a depth-dependent point spread function (PSF), based on which a scattering suppression method was proposed using transcutaneous fluorescent imaging to restore vein patterns. Similarly, some optical model [22]–[24] are employed to remove light scattering occurrence in biological tissue during imaging.

B. FEATURE LEVEL RESTORATION

In many finger-vein verification systems [4], [5], [13]–[16], the vein networks are extracted and stored in binary images as features. Then, the resulting binary images are employed

for matching. In general, the vein networks is not connective as the some vein patterns are missed during the image processing. So, in this category, the vein patterns instead of global images are restored for the visibility improvement of finger-vein images. Few approaches have been proposed to recover the vein network for verification. For example, in the existed methods [4], [13], [18], some filtering technology such as mathematical morphology and median filtering are employ to restore the segmented vein network. As these methods restore veins based on a distance metric, few missed veins are recover and some vein networks with a small corruption may be connected with each other. However, the missing vein patterns are not recovered in the images with a huge corruption. To overcome this problem, a Direction-Variance-Boundary Constraint Search (DVBCS) model is presented to restore the missed finger-vein patterns in work [25].

These image level restoration based methods only focus on the global images instead of only vein network, so some finger-vein patterns are still not restored and the connectivity of restoring vein network may be poor. The feature level restoration based approaches may alleviate the problem, but they restore the vein patterns based on the handcrafted descriptors and suffer follows problems. (1) The handcrafted based approaches are developed based on limited prior knowledge that might discard relevant information about vein restoration. (2) The handcrafted based approaches do not infer any knowledge from the different images as they restore each image independently from the others.

Recently, deep learning approaches without using handcrafted features have been directly used to learn robust feature from raw pixel images and have been applied for many computer vision tasks [5], [26]–[29]. These works imply that deep learning approaches circumvent the need of designing hand-crafted descriptors by automatically deriving robust feature representations for the task at hand. This is because a byproduct of deep learning models is a learning of suitable representations directly from raw input. Inspired by this idea, we develop, in this paper, a novel finger-vein restoration scheme based on generative adversarial network (GAN) to restore finger-vein patterns. This work makes the first attempt to accommodate GANs on the finger-vein pattern restoration. First, a baseline is employed to extract vein network and stored it in a binary image. Second, a generative adversarial network is built to restore the vein network. Third, the vein minutiae points are extracted from the resulting images and a matching approach of combining vein minutiae points and vein network is proposed to achieve the authentication. The experimental results show that the proposed approach can restore missed vein patterns and reduce the verification error.

In previous work [37], the GAN has been proposed to segment finger-vein network for verification. First, this work named FV-GAN makes first attempt to accommodate GANs on the finger-vein segmentation task. Second, FV-GAN is proposed based on CycleGAN [40]. The proposed FV-GAN consists of a pattern generator, an image generator and a discriminator. Different from the original CycleGAN, its

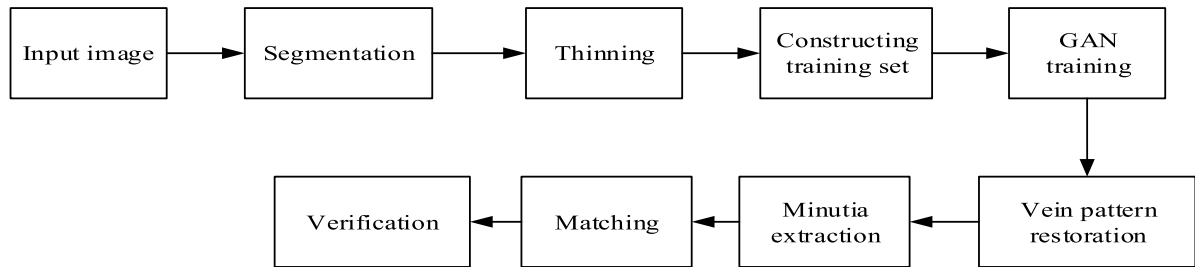


FIGURE 2. Proposed algorithm framework.

discriminator is designed to distinguish two generated vein patterns: One is generated by taking real vein image as input of the pattern generator and the other is produced by taking fake vein images as its input again. Third, instead of the L_1 loss, the focal loss is employed as the cycle consistency loss because the vein patterns in the latent space are binarized and the class imbalance exists in vein patterns. The proposed work has a different motivation and improves original GAN in significant ways. 1) Our work makes the first attempt to accommodate GANs on the finger-vein pattern restoration task instead of vein pattern segmentation. 2) FV-GAN is proposed based on CycleGAN and contains two generators, namely image generator and pattern generator and a discriminator. In our GAN, we develop a new fully convolutional network as the generator and a patch CNN as discriminator. In addition, instead of L_1 loss, the L_2 loss is employed as consistency loss to penalize distance between the ground truth and outputs. The experimental results imply that our model works well on vein restoration task. 3) Unlike FV-GAN which divide an image into several patches and construct a patch-based set for training, the entire finger-vein images and their corresponding ground truths are directly input into our GAN model for training. In the testing phase, the entire image is taken as input of GAN to restore vein pattern. Therefore, our approach takes into account localization and the use of global context at the same time. Moreover, it can directly recover binary vein patterns in one forward propagation without pre-processing and post-processing, which results in low-time cost.

II. THE PROPOSED FINGER-VEIN PATTERN RESTORATION METHOD

Some researchers have shown that the vein minutiae patterns, such as the endpoints and intersections, can represent the distinctive information to achieve effect verification. Also, using minutiae patterns for matching and verifying, the time cost and storage cost are low compared to other patterns such as vein network [13], [14], [16], [25]. Therefore, the minutiae patterns have been widely investigated and successfully employed for finger-vein verification. However, as the quality of finger-image is affected by many factors during the capturing process, there are some ambiguous regions where the separability between the vein and nonvein patterns is poor

or some corruption regions where vein patterns are missed. After image processing, many incorrect minutiae features are generated and matching them may degrade the verification accuracy. To overcome this problem, first, we extract the vein network using image segmentation approach and the resulting vein patterns are further thinned to obtain skeleton image. Then, a GAN model is built and trained. After training, we take skeleton image as an input of generator to restore vein patterns. Finally, the minutiae features are extracted from restoration image for matching. The framework of the proposed approach is shown in Fig.2.



FIGURE 3. Segmentation results: (a) original image; (b) segmentation image (c) skeleton image.

A. IMAGE SEGMENTATION AND THINNING

To verify the proposed vein pattern restoration approach, the vein patterns are extracted using existing segmentation methods [30]. The segmentation result is shown in Fig.3. Then, the vein patterns are thinned by mathematical morphology operation [13] and a skeleton image is obtained, as shown in Fig.3(c). The minutiae patterns can be extracted from skeleton image for matching. As there are some noises and ambiguous regions in Fig.3(a), the vein patterns are not connective in the segmentation image and skeleton image.

B. VEIN PATTERN RESTORATION

Based on the anatomy of finger skin (as shown in Fig.1), the vein network are clear and connective. However, as the quality of the capturing finger-vein image is affected by many factors, the vein patterns are easy to be corrupted (as shown in Fig.3(c)). In general, these corrupted images show poor connectivity because some vein patterns are missed, which results many incorrect minutiae patterns such as endpoint and bifurcation point. Matching such minutiae patterns comprises the verification performance. To overcome drawback, we propose a generative adversarial network to recover the vein patterns for verification. Firstly, given an image, an existing method is employed to segment the vein network and the resulting binary images are thinned to obtain skeleton images. Then, a generative adversarial network is built and trained

to restore the vein patterns. Finally, the minutiae patterns are extracted and matched for verification.

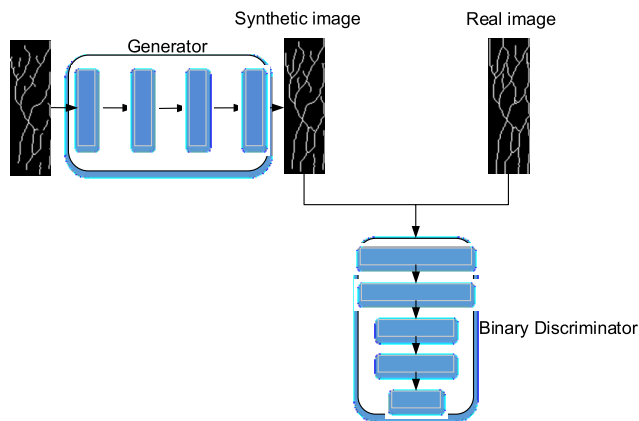


FIGURE 4. The proposed Generative Adversarial Networks (GANs) framework for vein pattern restoration.

C. GAN FRAMEWORK STRUCTURE

We develop a generative adversarial network (GAN) to recover the vein minutiae pattern, as shown in Fig.4. Our Generative Adversarial Networks (GANs) consist of generator and discriminator. Taking a skeleton image as an input of the generator, it generates probability maps with the same size as the input. Values in the probability maps range from 0 to 1 indicating the probability of being a pixel of vein pattern. The discriminator takes a vein image and ground truth to determine whether the vein image is the ground truth or output of the generator.

1) GENERATOR ARCHITECTURE

Our generator consists of two constitutional layers, a input layer and output layer. Fig.5 shows the architecture of our generator. The input is a corrupted finger-vein image x and the output is the finger-vein image with recovered missing patterns. In our experiments, both input and output layers are a matrix with size of 73×240 , respectively. The size of weight kernels in each layer is experimentally determined to 9×9 , 5×5 , and 3×3 , and the dimensions of the output in the layers are respectively set to $n_1 = 64$, $n_2 = 64$, and $n_3 = 1$ as shown in Fig.5. The output in each layer is padded such that reconstructed image and the ground truth have the same size. The convolutional layer in generator (as shown in Fig.5) can be denoted as follows.

Assuming x_m^l be the m -th input map of layer l . y_n^l is the n -th output map of layer l and computed as

$$y_n^l = \text{Relu}(\sum_m^{M^{l-1}} w_{n,m}^l * x_m^l + b_n^l) \quad (1)$$

where $*$ represents the convolutional operation, $w_{n,m}^l$ denotes the weights between the m -th input and the n -th output maps, M^{l-1} is the number of input maps, b_n^l is the bias of the n -th output map, and Relu is an activation function, named Rectified Linear Units ($y = \max(x, 0)$).

2) DISCRIMINATOR ARCHITECTURE

The discriminator network has a typical CNN architecture that takes the input image of size 73×240 and outputs one decision: is this a real pair (ground truth) or is it a fake pair (output of generator)? The network consists of three convolutional layers with a kernel size of 3×3 and one fully connection layer. To reduce spatial dimensionality, the Max pooling is applied to each convolution layer. Drop out is applied to two fully connection layers. The ReLU activation functions is applied to all layers except the output layer which uses the Sigmoid function for the likelihood probability score of the image.

3) OBJECTIVE FUNCTION

Let the generator G be a mapping from a hand image x to a vein image $G(x)$. Then, taking $G(x)$ as input, the discriminator D makes a binary decision $\{0,1\}$, where 0 or 1 represent that $G(x)$ is produced by the generator or is the ground truth, respectively. Adversarial networks are trained by optimizing the following loss function of a two-player minimax game.

$$L_{adv} = \mathbb{E}_{y \sim p_{data}(x,y)} [\log D(y)] + \mathbb{E}_{x \sim p_{data}(x)} [\log(1 - D(G(x)))] \quad (2)$$

where $\mathbb{E}_{y \sim p_{data}(y)}$ is the expectation over the y sampled from the joint data distribution of real pairs $p_{data}(y)$ and $\mathbb{E}_{x \sim p_{data}(x)}$ is the expectation over the x sampled from the real vein network distribution $p_{data}(x)$.

In fact, the recovery task can also utilize ground truth by adding loss functions that penalize distance between the ground truth and outputs. Here, the mean squared error is employed as loss function, which is defined by:

$$L_{rec} = \sum_{i=1}^n \|G(x) - y\|^2 \quad (3)$$

Summing up both the adversarial loss and the reconstruction loss, we can formulate the objective function as

$$L_{seg} = L_{adv}(G, D) + \lambda L_{rec} \quad (4)$$

To optimize our model, the gradient descent with Adam Optimizer is employed to minimize the loss function and then update the weight. The learning rate and the trade-off coefficient λ in Equation (4) is 0.0002 and 300.

D. TRAINING AND TEST OF GAN

To train our model, we generate a training set as follows. First, we employ existing approach to obtain the skeleton image and remove isolated regions that have fewer pixels than a threshold from the skeleton image. Second, some skeleton images with good connective vein patterns are selected as ground truth image. Third, to generate corrupted images, we randomly crop the ground truth images at different locations as shown in Fig.6. In this way, we generate multiple ground truth images and corrupted images to obtain a training set. The setup of training set is detailed in section IV.

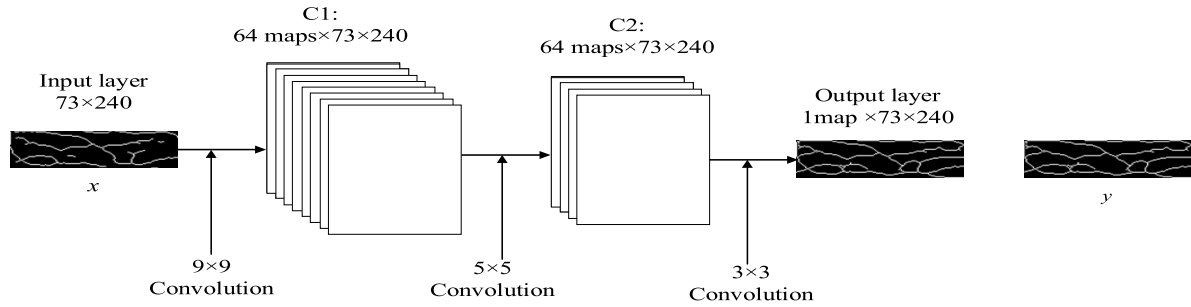


FIGURE 5. Architecture of generator.



FIGURE 6. Corruption image generation process: (a) ground truth; (b) corrupted image.



FIGURE 7. Minutiae pattern extraction: (a) skeleton image; (c) minutiae patterns from (a), which are marked in red color.

In the training stage, our GAN takes a pair of corruption image and ground truth image as input. The generator is responsible of producing r image samples, which has the same distribution as the ground truth. This is achieved through adversarial training, where generator learns to fool a discriminator, which attempts to distinguish the generated samples from ground truth. For testing, given an image either from a training or a test image, the generator outputs the restoration image.

III. MINUTIAE EXTRACTION AND MATCHING

A. MINUTIAE EXTRACTION

In fingerprint recognition, fingerprints can be represented by key points (ridged intersections and ridged endpoints) in the image. These key points are called minutiae points which are used to match the characteristics of a pair of fingerprints to identify a person [9], [10], [38]. Similarly, minutiae points that contain geometric information are employed for finger-vein verification in many existing works [13]–[16]. Therefore, we extract vein minutiae patterns by work [13] and match them for verification. Fig.7 has shown minutiae patterns extracted from a skeleton image.

B. MINUTIAE MATCHING

After extracting minutiae patterns, a vein image can be represented by a set of two-dimensional points. The Hausdorff distance is a natural similarity measure of the two point sets, so the vein image can be matched by a modified Hausdorff distance (MH) [31]. In past years, the MHD has been usually employed to match the vein minutia features [13]–[16] and achieve promising results. In addition, the template matching approach has also shown good performance in finger-vein verification [4], [5], [17]–[20]. To further improve verification accuracy, we combine the template matching with minutiae matching for vein verification.

1) MINUTIAE POINT MATCHING BASED ON Hausdorff

As a finger-vein minutiae point can be represented by a two-dimensional point set, we match two images by computing the Hausdorff similarity [32] between the two point sets. However, the original Hausdorff distance is very sensitive to the small sway of this point. Therefore, to solve this problem, work [31] proposed a modified Hausdorff distance for matching. Let $X = \{x_1, x_2, x_3, \dots, x_{N_x}\}$ and $Y = \{y_1, y_2, y_3, \dots, y_{N_y}\}$ be the two minutiae sets of the input image and the registered image, respectively and a modified Hausdorff distance is defined as follows.

$$HD(X, Y) = \max(d(X, Y), d(Y, X)) \quad (5)$$

$$d(X, Y) = \frac{1}{N_X} \sum_{x_i \in X} \min_{y_j \in Y} \|x_i - y_j\| \quad (6)$$

2) TEMPLATE MATCHING BASED ON Hausdorff

As the finger-vein minutiae pattern are susceptible to noise, the matching accuracy still is limited by the Hausdorff distance. So, a Hausdorff based template matching method is proposed to improve verification performance and detailed as follows.

Suppose that there are two sets $X = \{x_1, x_2, x_3, \dots, x_{N_x}\}$ and $Y = \{y_1, y_2, y_3, \dots, y_{N_y}\}$ extracted from the test image and registered image, respectively and the matching distance between them is computed by

$$d(x_i, y_i^*) = \min_{y_j \in Y} \|x_i - y_j\| \quad (7)$$

Each x_i corresponds a matching point y_i^* , so there are N_x matching pairs associated with N_x distance. To enhance matching performance, K ($K \leq N_x$) matching pairs associated with the K smallest distances are stored and denoted as $X' = \{x'_1, x'_2, x'_3, \dots, x'_K\}$ and $Y' = \{y'_1, y'_2, y'_3, \dots, y'_K\}$. A and B respectively represent vein patterns extracted from the test image and registered image. Based on K matching

pairs, the K sub-regions A' and B' from A and B are denoted as follows.

$$A' = \left\{ a_k^{w_a, h_a} \mid a_k^{w_a, h_a} \in A, k = 1, 2, \dots, K \right\} \quad (8)$$

$$B' = \left\{ b_k^{w_b, h_b} \mid b_k^{w_b, h_b} \in B, k = 1, 2, \dots, K \right\} \quad (9)$$

where $a_k^{w_a, h_a}$ and $b_k^{w_b, h_b}$ is a pair of matching sub-regions separated from A and B . w_a and h_a are the width and height of sub-region $a_k^{w_a, h_a}$, w_b and h_b are the width and height of the sub-region $b_k^{w_b, h_b}$, and $w_a > w_b$, $h_a > h_b$. Note that the matching sub-regions $a_k^{w_a, h_a}$ and $b_k^{w_b, h_b}$ centers at k th matching minutiae points x'_k and y'_k . So, the matching scores of A and B is obtained by.

$$S(A, B) = S(A', B') = \frac{1}{K} \sum_{k=1}^K \Psi_k \quad (10)$$

where Ψ_k is the matching score of two corresponding sub-regions and is defined as (11), as shown at the bottom of the page, where p and q are the translation in the horizontal and vertical directions, respectively, and Φ is defined as follows.

$$\Phi(P_1, P_2) = \begin{cases} 1 & \text{if } |P_1 - P_2| = 1 \\ 0 & \text{otherwise} \end{cases} \quad (12)$$

where P_1 and P_2 are the pixel values of the input image and registered image, respectively.

3) FUSING MATCHING SCORES

To improve the matching accuracy, we combine the matching score of minutiae point with the template matching score to generate the final matching score $D(X, Y)$ which is computed as follows.

$$D(X, Y) = \frac{1}{2} (HD(X, Y) + S(A, B)) \quad (13)$$

IV. EXPERIMENTS AND ANALYSIS

To evaluate the performance of the proposed approach for finger-vein verification, we carry out experiments on a realistic databases. The baseline [30] is employed to extract the finger-vein network patterns and the resulting vein patterns are recovered by the proposed approach. Then, the minutiae features are extracted from the recovering image for verification. Also, the minutiae feature restoration approaches [12], [25] are employed to recover the vein patterns and the verification results are reported in our comparable experiments. We train our model using anaconda and tensorflow on the Ubuntu system of 16G memory and GeForce GTX 1080ti GPU, and calculate the equal error rate (EER) before and after restoring in matlab2016b.

A. DATABASE

To evaluate the proposed approach, we carried experiments on two public finger-vein databases.

1) DATABASE A

The database MMCBNU_6000 [7] which is collected from Chonbuk National University in Korea are employed in our experiments. The database contains 100 students or teachers from 20 countries including Asia, Europe, Africa and the United States, whose ages range from 16 to 72 years old. As the length of the thumb and the little finger is too short, they collected the index finger, median and ring finger of each individual's right and left hands, and every fingers 10 times. Therefore, the database contains 100 subjects \times 6 fingers \times 10 samples = 6000 images, and each image pixel is 640 \times 480 (shown in Fig.8(a)). As the background region does not include any discriminative information, we crop it and resize the resulting image to 73 \times 240. The preprocessing images are shown in Fig.8(b).

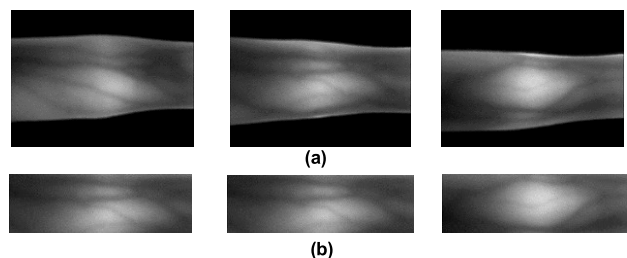


FIGURE 8. Finger-vein image samples.(a) original finger-vein images samples;(b) the preprocessing finger-vein image samples.

2) DATABASE B

USM database [8] includes 5904 images from 123 subjects, collected at two different sessions. Each subject provided two fingers, e.g. index and middle fingers, which results in a total of 492 finger class. In each session, each finger provided 6 images and thus 2952 (492 \times 6) images are collected. So, there are a total of 5904 images for at two sessions. All images are subject to preprocessing and normalized to 70 \times 210.

B. EXPERIMENTS SETTING

To verify the proposed approach, we divide the database into three sub-datasets for training, validation and testing, respectively. For database A, there are 100 subjects associated with 600 fingers, each of which provides 10 images. The different fingers of the same hand are treated as different classes, based on which we split the database into three sets: training dataset with 2000 (200 fingers \times 10 images) images, validation dataset with 2000 (200 fingers \times 10 images) images and test dataset with 2000 (200 fingers \times 10 images) images. To simplify the description, the three datasets are presented as

$$\Psi_k = \min_{\forall x \in [0, w_a - w_b], y \in [0, h_a, h_b]} \frac{\sum_{u=0}^{w_b-1} \sum_{v=0}^{h_b-1} \Phi(a_k^{w_a, h_a}(u+p, v+q), b_k^{w_b, h_b}(u, v))}{w_b \times h_b} \quad (11)$$

dataset A1, A2 and A3, respectively. For database B, there are 123 subjects associated with 492 fingers. Similarly, there are 1476 images (123 fingers × 12 images) in the training dataset, 1476 images (123 fingers × 12 images) in the validation dataset, and 2952 images (246 fingers × 12 images) in the test dataset, which is denoted as dataset B1, B2, and B3. To effectively verify our approach, the test datasets A3 and B3 consists of low quality images where the connectivity of vein patterns is poor.

To generate ground truth image, the existing approaches [30] are employed to segment the finger-vein image in training set (A1 or B1) and the resulting network patterns are further thinned to obtain skeleton image. Then, we filter some isolated regions that have fewer pixels than a threshold from the skeleton image and the resulting finger-vein image is determined as ground truth image (As shown in Fig.9(a)). To generate corruption image, we randomly crop the ground truth image at different locations (As shown in Fig.9(b)). Therefore, we obtain 100000 corruption images and their corresponding ground truth images in this way. For each ground truth image, there are about 50 and 70 corrupted images for datasets A1 and B1, respectively. The GAN is trained based on the corrupted image and its ground truth image.

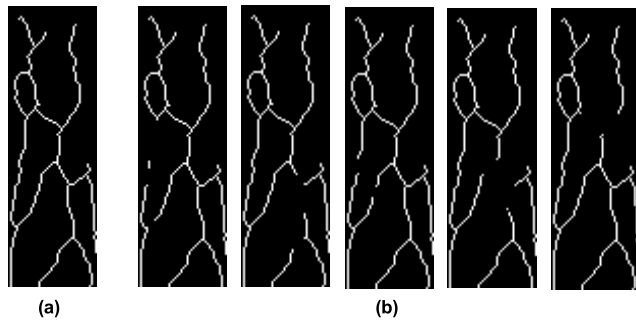


FIGURE 9. Corruption image samples: (a) thinning image; (b) corruption image.

C. PARAMETER SELECTION

After training, we input a testing image into generator and its output is a restoration image. If such an output is fed back as input to the generator again, there are more vein patterns to be restored, which enable the restoring to be done in a recursive way. The number of iteration steps is key to achieve high verification accuracy. The small number of iteration steps may result that some missed vein patterns are not restored. So, there are still incorrect minutia patterns in restoration image. By contrast, if the number of iteration steps is large, some non-vein patterns may be wrongly generated, which also results minutia patterns. In our experiments, we employ approaches [30] to extract the vein network and obtain the skeleton image. The vein patterns skeleton image are restored at different numbers of iterative steps. We extract the minutia features and compute the matching score by Equation (13). Then, the images from first session are used for training and remaining ones for testing for each finger. For verification

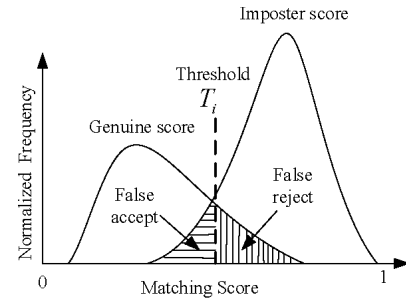


FIGURE 10. Genuine and imposter distributions [35].

set A2, there are 200 fingers with 2000 images. We match images from same finger and different fingers to generate 1000 (200 × 5) genuine scores and 199000 (200 × 199 × 5) imposter scores, based on which we compute the false rejected error (*FRR*) and false accepted error (*FAR*). The *FAR* and *FRR* [35] are detailed as follows. First, we denote *T* as a set which is sampled from 0 to 1 at sampling interval of 0.0001, namely $T = \{0, 0.0001, 0.0002, \dots, 0.9999, 1\}$. So there are 10001 elements in set *T*, where T_i is the *i*th threshold in set *T*. Assume that there are genuine score set and imposter score set, which are denoted as *GS* and *IS*, respectively. If the score is lower than the predefined decision threshold T_i , then the claimant is accepted by the verification system, otherwise the claimant is rejected. As shown in Fig.10, the area under the genuine score distribution above a chosen threshold T_i , is the false rejected score set and represented as *FR*, while the area under the imposter score distribution below the threshold T_i , is the false accepted score set and denoted as *FA*. FAR_i and FRR_i are *FAR* and *FRR* at threshold T_i , and computed by

$$FRR_i = \frac{\text{Number of matching scores in FR}}{\text{Number of matchings cores in GS}} \quad (14)$$

$$FAR_i = \frac{\text{Number of matching scores in FA}}{\text{Number of matching scores in IS}} \quad (15)$$

So, there is a pair of *FAR* and *FRR* for each threshold. The *FAR* will increase and *FRR* will reduce when threshold T_i increases from 0 to 1. By contrast, the decreasing threshold will result in low *FAR* and high *FRR*. The equal error rate (*EER*) is the error when *FAR* is equal to *FRR*, namely $EER = FRR_{i^*} = FAR_{i^*}$. The Genuine accept rate (*GAR*) is computed as

$$GAR_i = 1 - FRR_i \quad (16)$$

Receiver operating characteristics (*ROC*) curves [36], [39] are two-dimensional curves in which true positive rate is plotted on the *Y* axis and false positive rate is plotted on the *X* axis. An *ROC* graph implies relative tradeoffs between benefits (true positives) and costs (false positives). In our experiment, the *ROC* curve is obtained by plotting GAR_i versus FAR_i at varying the threshold T_i .

The results of *EER* are shown in Fig.11. From Fig.11, we can see that the lowest *EER* is achieve when the numbers of the iteration step is 5. Therefore, we set the number of

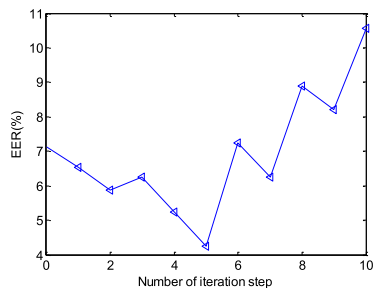


FIGURE 11. The EER at different number of iteration step.

the iteration to 5 for database A. As the thinning images from database A and database B is very similar, the number of iteration is also determined to 5 for database B in our experiments.

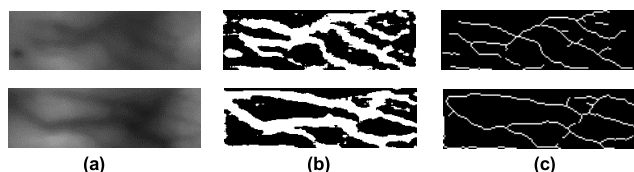


FIGURE 12. Segmentation and thinning results: (a) original image; (b) segmentation image; (c) thinning image.

D. VISUAL ASSESSMENT

In this section, we visually analyze the restoring vein patterns from our approach to get more insights into the proposed approach. We use segmentation algorithm [30] to extract vein network patterns and the resulting image is subject to thinning, as shown in Fig.12. Further, the thinning image (skeleton image) is taken as an input of GAN to restore vein pattern. The restoration image is shown in Fig.13. After one iteration, the proposed model can restore few missing vein patterns. More vein patterns are restored with an increasing number of iterations. After 9 iterations, the restoration vein patterns have very good connectivity. Also, we can see that the missing vein patterns are naturally restored in spite of a huge corruption in the input finger-vein image. In Fig.13, we also show the false minutia with high probability and mark them in red color. The number of false minutia decreases with the increasing iteration number. In other words, the correct minutia features will be generated when the missed vein patterns are restored, which may improve the matching accuracy of vein verification. These experimental results imply that, by learning the underlying structure of labeled cropped vein patterns on a huge dataset, the GAN is able to generalize over unknown and unlabeled missing vein pattern for restoration.

E. VERIFICATION RESULTS

In this section, we evaluate the performance of finger-vein verification approach [10] and show how much it can be improved by adopting our approach to restoration. Also, the restoration approaches [12], [25] are employed to restore vein pattern and the verification results are reported for

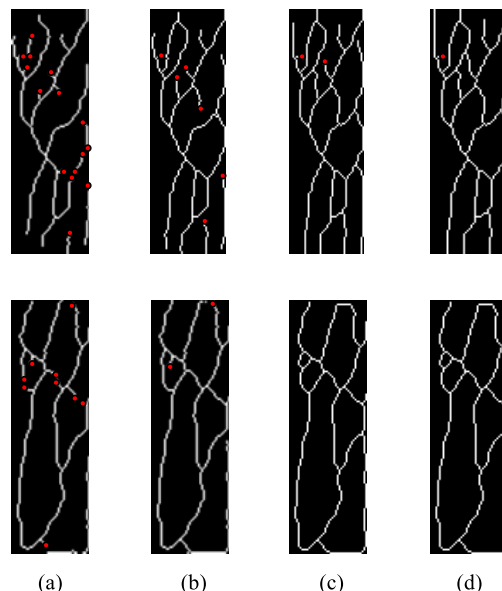


FIGURE 13. Restoration image: (a) original image; (b) restoration image (iteration = 1 times); (c) restoration image (iteration = 5 times); (d) restoration image (iteration = 9 times), where the red points presents the false minutia features.

comparison. In our experiment, we employ [30] to extract vein pattern and obtain the skeleton image. Then, the vein patterns are restored by our approach and existing approach. Finally, the minutia features are extracted and matched for verification. The EER of the system [30] before and after automatically restoring the vein patterns is calculated to get insight on finger-vein verification. In addition, as two descriptors of LBP [33] and SIFT [34] have achieved high performance on finger-vein verification, we report their verification accuracy in comparable experiments. In the testing set A3, there are 2000 images (200 fingers \times 10 images) from 200 fingers. Matching images from the same finger generate genuine scores while the impostor scores are created by matching images from different hands. As a result, there are 9000 (45 \times 200 fingers) genuine scores. Computing the impostor matching score is time consuming because there are 178, 200 (10 \times 10 \times 200 \times 199 / 2) matching groups. To reduce computation cost, we randomly split all fingers into 10 groups and then compute impostor matching scores for each group. For example, the 200 fingers in test set is split into 10 groups and each group includes 200 (10 \times 20) images from 20 fingers. For each group, matching the i -th sample from different fingers ($i = 1, 2, 3, 4, 5, 6, 7, 8, 9, 10$) generates 1900 (20 \times 19 \times 5) impostor matching scores. So, there are totally 19000 (1900 \times 10 groups) impostor matching scores for 10 groups. For testing dataset B3, 2952 images from 246 fingers are employed for verification. Similarly, 1476 (246 \times 6) genuine scores and 59040 (41 \times 40 \times 6 \times 6 groups) impostor matching scores are produced from dataset B3. The verification results for database A and database B are listed in Table 1 and corresponding ROC curve is showed in Fig.14.

TABLE 1. EER from various approaches.

Methods	Database	Database B
	A	
The segmentation algorithm [30]	7.96	4.95
The restoration approach [25]	6.51	3.79
The restoration approach [12]	7.41	4.34
The proposed restoration approach	5.66	2.37
LBP[33]	8.41	5.89
SIFT[34]	11.23	7.11

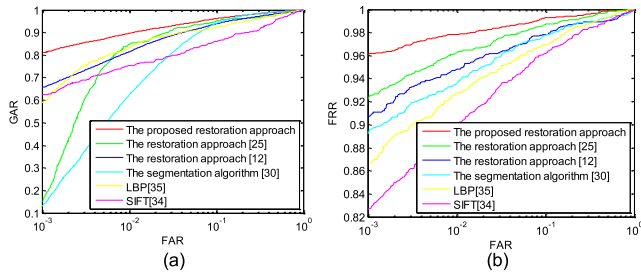


FIGURE 14. Receiver operating characteristics from (a) database A and database B.

We observe from Fig.14 and Table 1 that the proposed approach using a GAN deep representation achieves the best performance among all the approaches considered in this work. The baseline achieves the higher EERs of 7.96% and 4.95% on the dataset A and database B, respectively. For two handcrafted based restoration methods [12], [25], after restoring the vein patterns of images in database A, the ERR decreases lower than 7.5 %, and the EER is reduced to 5.66% when adopting the proposed restoration approach. For database B, the proposed approach outperforms restoration methods [12], [25] and achieve lowest EER of 2.37%. Compared to the verification error before restoration, the performance is significantly improved after the missing patterns are recovered by our model. For example, the EER (Table 1) is reduced from 7.96% to 5.66% (about 28.89% relative error reduction) for database A. For database B, a lower EER, namely 2.37% (about 52.12% relative error reduction) is achieved by the proposed approach. The ROC curve shows the similar trend that the proposed approach outperforms the existing handcrafted approaches and significantly reduces the verification error of the finger-vein recognition system.

From Table 1, we also observe that the baseline segmentation algorithm [30] achieve higher verification accuracy on database B compared to results on database A, but the proposed approach still improve accuracy. In addition, the LBP descriptor [33] and SIFT descriptor [34] do not achieve promising verification accuracy on two public databases, which can be explained that the finger-vein image contains less local feature points because vein patterns are non-rigid, round and smooth objects.

Overall, the finger-vein verification accuracy on the two datasets is improved by restoring the missing vein patterns, which implies the restoration vein features can contribute more discriminative information for verification. Such a good

performance can be explained by following fact: (1) The proposed approach learns a rich prior knowledge acquired by training on a huge image set from different images so that it is capable of restoring the missed vein pattern. (2) The GAN takes as input the image to uncover hierarchical features in such a way to minimize its decision errors on vein patterns, so it avoids the need of first explicitly extracting some image processing-based features that might discard relevant information about vein restoration.

V. CONCLUSIONS

In this paper, a GAN based restoration algorithm is proposed to recover the missed vein pattern. The proposed scheme does not rely on hand-crafted features and directly learn robust feature representations from the vein image. The experimental results show that the proposed algorithm is capable of restoring the finger-vein pattern to improve the verification accuracy of finger-vein recognition. In addition, the method can be used for pattern restoration of other images, such as fingerprints and palm-print images.

REFERENCES

- [1] J. J. Engelsma, S. S. Arora, A. K. Jain, and N. G. Paulter, "Universal 3D wearable fingerprint targets: Advancing fingerprint reader evaluations," *IEEE Trans. Inf. Forensics Security*, vol. 13, no. 6, pp. 1564–1578, Jun. 2018.
- [2] R. He, X. Wu, Z. Sun, and T. Tan, "Wasserstein CNN: Learning invariant features for NIR-VIS face recognition," *IEEE Trans. Pattern Anal. Mach. Intell.*, vol. 41, no. 7, pp. 1761–1773, Jul. 2019.
- [3] C. Wang, J. Muhammad, Y. Wang, Z. He, and Z. Sun, "Towards complete and accurate iris segmentation using deep multi-task attention network for non-cooperative iris recognition," *IEEE Trans. Inf. Forensics Security*, vol. 15, pp. 2944–2959, Mar. 2020.
- [4] W. Kang, H. Liu, W. Luo, and F. Deng, "Study of a full-view 3D finger vein verification technique," in *IEEE Trans. Inf. Forensics Security*, vol. 15, pp. 1175–1189, 2020, doi: 10.1109/TIFS.2019.2928507.
- [5] H. Qin and M. A. El-Yacoubi, "Deep representation-based feature extraction and recovering for finger-vein verification," *IEEE Trans. Inf. Forensics Security*, vol. 12, no. 8, pp. 1816–1829, Aug. 2017.
- [6] L. Yang, G. Yang, X. Xi, X. Meng, C. Zhang, and Y. Yin, "Tri-branch vein structure assisted finger vein recognition," *IEEE Access*, vol. 5, pp. 21020–21028, 2017.
- [7] Y. Lu, S. Xie, S. Yoon, J. Yang, and D. Park, "Robust finger vein ROI localization based on flexible segmentation," *Sensors*, vol. 13, no. 11, pp. 14339–14366, Oct. 2013.
- [8] M. S. M. Asaari, S. A. Suandi, and B. A. Rosdi, "Fusion of band limited phase only correlation and width centroid contour distance for finger based biometrics," *Expert Syst. Appl.*, vol. 41, no. 7, pp. 3367–3382, Jun. 2014.
- [9] A. Nagar, K. Nandakumar, and A. K. Jain, "A hybrid biometric cryptosystem for securing fingerprint minutiae templates," *Pattern Recognit. Lett.*, vol. 31, no. 8, pp. 733–741, Jun. 2010.
- [10] T.-Y. Jea and V. Govindaraju, "A minutia-based partial fingerprint recognition system," *Pattern Recognit.*, vol. 38, no. 10, pp. 1672–1684, Oct. 2005.
- [11] A. Kavipriya and A. Muthukumar, "New insights on finger knuckle print identification with steerable filter for faster and accurate matching," in *Proc. IEEE Int. Conf. Intell. Techn. Control, Optim. Signal Process. (INCOS)*, Tamilnadu, India, Apr. 2019, pp. 1–5.
- [12] A. Kumar and B. Wang, "Recovering and matching minutiae patterns from finger knuckle images," *Pattern Recognit. Lett.*, vol. 68, pp. 361–367, Dec. 2015.
- [13] C.-B. Yu, H.-F. Qin, Y.-Z. Cui, and X.-Q. Hu, "Finger-vein image recognition combining modified Hausdorff distance with minutiae feature matching," *Interdiscipl. Sci. Comput. Life Sci.*, vol. 1, no. 4, pp. 280–289, Dec. 2009.
- [14] L. Wang, G. Leedham, and D. S.-Y. Cho, "Minutiae feature analysis for infrared hand vein pattern biometrics," *Pattern Recognit.*, vol. 41, no. 3, pp. 920–929, Mar. 2008.

- [15] L. Yang, G. Yang, Y. Yin, and X. Xi, "Finger vein recognition with anatomy structure analysis," *IEEE Trans. Circuits Syst. Video Technol.*, vol. 28, no. 8, pp. 1892–1905, Aug. 2018.
- [16] F. Liu, G. Yang, Y. Yin, and S. Wang, "Singular value decomposition based minutiae matching method for finger vein recognition," *Neurocomputing*, vol. 145, pp. 75–89, Dec. 2014.
- [17] H. Qin and M. A. El-Yacoubi, "Deep representation for finger-vein image-quality assessment," *IEEE Trans. Circuits Syst. Video Technol.*, vol. 28, no. 8, pp. 1677–1693, Aug. 2018.
- [18] L. Yang, G. Yang, X. Xi, K. Su, Q. Chen, and Y. Yin, "Finger vein code: From indexing to matching," *IEEE Trans. Inf. Forensics Security*, vol. 14, no. 5, pp. 1210–1223, May 2019.
- [19] W. Kang, Y. Lu, D. Li, and W. Jia, "From noise to feature: Exploiting intensity distribution as a novel soft biometric trait for finger vein recognition," *IEEE Trans. Inf. Forensics Security*, vol. 14, no. 4, pp. 858–869, Apr. 2019.
- [20] B. Prommegger, C. Kauba, M. Linortner, and A. Uhl, "Longitudinal finger Rotation–Deformation detection and correction," *IEEE Trans. Biometrics, Behav., Identity Sci.*, vol. 1, no. 2, pp. 123–138, Apr. 2019.
- [21] W. Kim, "Vein enhancement using a dark diffusion prior," *IEEE Signal Process. Lett.*, vol. 25, no. 9, pp. 1325–1329, Sep. 2018.
- [22] J. Yang, B. Zhang, and Y. Shi, "Scattering removal for finger-vein image restoration," *Sensors*, vol. 12, no. 3, pp. 3627–3640, Mar. 2012.
- [23] J. Yang and Y. Shi, "Towards finger-vein image restoration and enhancement for finger-vein recognition," *Inf. Sci.*, vol. 268, pp. 33–52, Jun. 2014.
- [24] J. Choi, K. J. Noh, S. W. Cho, S. H. Nam, M. Owais, and K. R. Park, "Modified conditional generative adversarial network-based optical blur restoration for finger-vein recognition," *IEEE Access*, vol. 8, pp. 16281–16301, 2020.
- [25] T. Liu, J. Xie, W. Yan, P. Li, and H. Lu, "Finger-vein pattern restoration with direction-variance-boundary constraint search," *Eng. Appl. Artif. Intell.*, vol. 46, pp. 131–139, Nov. 2015.
- [26] Y. Taigman, M. Yang, M. Ranzato, and L. Wolf, "DeepFace: Closing the gap to human-level performance in face verification," in *Proc. IEEE Conf. Comput. Vis. Pattern Recognit.*, Jun. 2014, pp. 1701–1708.
- [27] Y. Sun, X. Wang, and X. Tang, "Deeply learned face representations are sparse, selective, and robust," in *Proc. IEEE Conf. Comput. Vis. Pattern Recognit.*, Jun. 2015, pp. 2892–2900.
- [28] D. C. Cireşan, U. Meier, L. M. Gambardella, and J. Schmidhuber, "Deep, simple neural nets for handwritten digit recognition," *Neural Comput.*, vol. 22, no. 12, pp. 3207–3220, Dec. 2010.
- [29] P. Isola, J.-Y. Zhu, T. Zhou, and A. A. Efros, "Image-to-image translation with conditional adversarial networks," in *Proc. IEEE Conf. Comput. Vis. Pattern Recognit.*, Jul. 2017, pp. 5967–5976.
- [30] H. Qin and X. Liu, "Finger vein image segmentation based on sparse auto-encoder," *J. Chongqing Technol. Bus. Univ. (Nat. Sci. Ed)*, vol. 36, no. 4, pp. 1–8, Aug. 2019.
- [31] M. P. Dubuisson and A. K. Jain, "A modified Hausdorff distance for object matching," in *Proc. 12th Int. Conf. Pattern Recognit.*, 1994, pp. 566–568.
- [32] W. J. Ruchlidge, "Efficiently locating objects using Hausdorff distance," *Int. J. Comput. Vis.*, vol. 24, pp. 251–270, Sep. 1997.
- [33] G. Sujani and G. M. S. Reddy, "A hierarchical finger selection method for finger vein recognition using sift," in *Proc. Int. Conf. Smart Technol. Smart Nation (SmartTechCon)*, Bengaluru, India, Aug. 2017, pp. 984–988.
- [34] E. C. Lee, H. Jung, and D. Kim, "New finger biometric method using near infrared imaging," *Sensors*, vol. 11, no. 3, pp. 2319–2333, Feb. 2011.
- [35] H. Qin, X. He, X. Yao, and H. Li, "Finger-vein verification based on the curvature in radon space," *Expert Syst. Appl.*, vol. 82, pp. 151–161, Oct. 2017.
- [36] T. Fawcett, "An introduction to ROC analysis," *Pattern Recognit. Lett.*, vol. 27, no. 8, pp. 861–874, Jun. 2006.
- [37] W. Yang, C. Hui, Z. Chen, J.-H. Xue, and Q. Liao, "FV-GAN: Finger vein representation using generative adversarial networks," *IEEE Trans. Inf. Forensics Security*, vol. 14, no. 9, pp. 2512–2524, Sep. 2019.
- [38] H. Kasban, "Fingerprints verification based on their spectrum," *Neurocomputing*, vol. 171, pp. 910–920, Jan. 2016.
- [39] N. A. Macmillan and C. D. Creelman, "Triangles in ROC space: History and the of 'nonparametric' measures of sensitivity and response bias," *Psychonomic Bull. Rev.*, vol. 3, no. 2, pp. 164–170, Jun. 1996.
- [40] J.-Y. Zhu, T. Park, P. Isola, and A. A. Efros, "Unpaired image-to-image translation using cycle-consistent adversarial networks," 2017, *arXiv:1703.10593*. [Online]. Available: <http://arxiv.org/abs/1703.10593>



SHUQIANG YANG received the B.Sc. degree from Luoyang Normal University, in 2000, and the M.Sc. degree from the Chongqing University of Technology, in 2009. He is currently an Associate Professor with the School of Physics and Electronic Information, Luoyang Normal University. His main research interests include signal acquisition and processing, the IoT wireless networks, automotive electronics, automatic control, and biometric recognition.



HUAFENG QIN received the B.Sc. degree from the School of Mathematics and Physics and the M.Eng. degree from the College of Electronic and Automation, Chongqing University of Technology, and the Ph.D. degree from the College of Opto-Electronic Engineering, Chongqing University. He is currently a Postdoctoral Researcher with the Department of Electronics and Physics, Telecom-SudParis, France. He is also a Professor with the School of Computer Science and Information Engineering, Chongqing Technology and Business University, China. His research interests include biometrics (e.g., vein and face) and machine learning.



XIA LIU received the B.S. degree in engineering from Chengdu Neusoft University, in 2015, and the M.S. degree in management from Chongqing Technology and Business University, in 2019. She is currently a Teacher with the School of Big Data and Software, College of Mobile Telecommunications, Chongqing University of Posts and Telecommunications. Her research interests include deep learning and biometric recognition.



JUN WANG received the B.S., M.S., and Ph.D. degrees in control theory and control engineering from the China University of Mining and Technology, Jiangsu, China, in 2003, 2009, and 2015, respectively. He was with the Jiangsu Province Laboratory of Electrical and Automation Engineering for Coal Mining. He has been an Associate Professor with the School of Information and Electrical Engineering, China University of Mining and Technology. His current research interests include intelligent control system design, computer vision, and pattern recognition, especially on vein recognition and other biometrical identification methods.

...